University of Massachusetts Medical School

eScholarship@UMMS

Open Access Articles

Open Access Publications by UMMS Authors

2019-07-24

Nonnative structure in a peptide model of the unfolded state of SOD1: Implications for ALS-linked aggregation

Noah R. Cohen
University of Massachusetts Medical School

Et al.

Let us know how access to this document benefits you.

Follow this and additional works at: https://escholarship.umassmed.edu/oapubs

Part of the Amino Acids, Peptides, and Proteins Commons, Biochemistry Commons, Biophysics Commons, Enzymes and Coenzymes Commons, Genetic Phenomena Commons, Molecular and Cellular Neuroscience Commons, Molecular Biology Commons, Nervous System Diseases Commons, and the Structural Biology Commons

Nonnative structure in a peptide model of the unfolded state of superoxide dismutase 1 (SOD1): Implications for ALS-linked aggregation

Noah R. Cohen[1], Jill A. Zitzewitz[1], Osman Bilsel[1], and C. Robert Matthews[1*]

From the [1]Department of Biochemistry and Molecular Pharmacology, University of Massachusetts Medical School, Worcester MA 01605

Running Title: *Non-native structure in the C-terminus of SOD1*

*To whom correspondence should be addressed: C. Robert Matthews: Department of Biochemistry and Molecular Pharmacology, University of Massachusetts Medical School, 364 Plantation St LRB 928, Worcester MA 01605; c.robert.matthews@umassmed.edu; Tel. 508-856-2251

Abstract

Dozens of mutations throughout the sequence of the gene encoding superoxide dismutase 1 (SOD1) have been linked to toxic protein aggregation in the neurodegenerative disease amyotrophic lateral sclerosis (ALS). A parsimonious explanation for numerous genotypes resulting in a common phenotype would be mutation-induced perturbation of the folding free-energy surface that increases the populations of high-energy states prone to aggregation. The absence of intermediates in the folding of monomeric SOD1 suggests that the unfolded ensemble is a potential source of aggregation. To test this hypothesis, here we dissected SOD1 into a set of peptides end-labeled with FRET probes to model the local behavior of the corresponding sequences in the unfolded ensemble. Using time-resolved FRET, we observed that the peptide corresponding to the loop VII-β8 sequence at the SOD1 C-terminus was uniquely sensitive to denaturant. Utilizing a two-dimensional form of maximum entropy modeling, we demonstrate that the sensitivity to denaturant is the surprising result of a two-state-like transition from a compact to an expanded state. Variations of the peptide sequence revealed that the compact state involves a nonnative interaction between the disordered N-terminus and the hydrophobic C-terminus of the peptide. This nonnative intramolecular structure could serve as a precursor for intermolecular association and result in aggregation associated with ALS. We propose that this precursor would provide a common molecular target for therapeutic intervention in the dozens of ALS-linked SOD1 mutations.

Introduction

Amyotrophic Lateral Sclerosis (ALS) is a neurodegenerative disorder affecting motor neuron cells, where it causes progressive loss of muscle control and eventual death (1, 2). Patients afflicted with ALS often only survive 2-3 years after the initial onset of symptoms, demonstrating the rapid and invariably fatal effects of the disease. The majority of all ALS cases occur in a sporadic nature, and only a small fraction (~10%) are linked to heritable mutations (1, 2). The first of the familial ALS proteins to be discovered was Cu,Zn superoxide dismutase (SOD1) (3). SOD1 is a homodimeric protein in which each monomer is comprised of a 153-residue chain that adopts a β-sandwich fold. Each monomer is stabilized by an intramolecular disulfide bridge and contains two metal ion cofactors, zinc and copper (Fig. 1A). The zinc ion has been shown to stabilize the protein, while the copper ion is crucial to the enzymatic activity of SOD1 (4). Intriguingly, >170 mutations in the *sod1* gene linked to ALS are located throughout the sequence of the protein (http://alsod.iop.kcl.ac.uk/) (5).

Although the mechanism of pathogenesis by mutations in SOD1 is poorly understood, a hallmark of ALS and many other

neurodegenerative diseases is the observation of large protein-rich aggregates in affected tissues (6). The observation of a common endpoint of large cellular inclusions has given rise to the hypothesis that ALS may result from toxicity related to protein misfolding and subsequent aggregation (7, 8). While the disulfide-intact, metal-bound SOD1 dimer is remarkably stable and resistant to aggregation (9), mutations are known to destabilize the native dimer and increase the populations of folded and unfolded forms of the monomeric protein that may nucleate aggregation (10–14). Several studies have suggested specific structures for such misfolded monomers and nonnative dimers (15–18). However, the large number of ALS-linked SOD1 mutations and, in particular, their distribution throughout the sequence, motivated us to propose a general explanation for the aggregation phenomenon.

Work from our lab on ALS variants of SOD1 have revealed that: (A) the destabilization of the metal-free native dimeric state increases the populations of both the folded and unfolded forms of the monomer (10), (B) the unfolded form of the disulfide-reduced monomer is favored at physiological temperatures (19), and (C) the lifetime of the unfolded monomer, prior to folding, is remarkably long, >10 s (20). These observations support the hypothesis that the unfolded form of SOD1, after synthesis on the ribosome and prior to folding and maturation, is the source of aggregation in motor neurons. Also supporting this hypothesis are the results of Lang *et al.* (21) which showed that the lag time prior to fibrillar aggregation of SOD1 *in vitro* was linked to the magnitude of population of SOD1 in the unfolded state. Increasing the unfolded state population with denaturant led to a decrease in the lag time and increase in the fibrillation rate, implicating the unfolded state as a common precursor for the aggregation of ALS variants. This work was expanded upon by comparison of the calculated *in vitro* aggregation rates to the *in vivo* aggregation rates determined for several mouse models (22). The good agreement argues for a common mechanism of aggregation *in vitro* and *in vivo*.

Eisenberg and colleagues have found that two heptapeptides derived from SOD1, one from the loop between β6-β7 and the other from β8, are capable of forming cross-beta structures that could serve as precursors to large scale aggregates (23).

The concept that discrete segments of SOD1 could serve as critical nucleation sites is further supported by the results of proteolytic digestion experiments on *in vitro* and *in vivo* derived aggregates of SOD1 (24). Three different continuous segments of SOD1, spanning β1-β3 (an interlocking pair of β-hairpins), β5-β6 (a β-hairpin) and Loop VII-β8 (a region that lacks native self-contacts) were shown to be strongly protected against proteolysis *in vitro*; *in vivo*, only the Loop VII-β8 segment was protected.

Building upon these results, we investigated the propensity for spontaneous collapse in five peptides that span the entire sequence of SOD1. We found that only the peptide corresponding to the Loop VII-β8 segment of SOD1 was capable of adopting a compact structure. Surprisingly, the compact form is separated from the expanded form by an energy barrier that gives rise to an apparent two-state behavior when exposed to increasing concentrations of denaturant, rather than a gradual swelling of the segment as would be expected for a randomly collapsed state. We propose that the Loop VII-β8 segment as a promising candidate to be the primary nucleation site for the aggregation of ALS variants of SOD1 in ALS.

Results
Strategy
We adopted the time-resolved FRET (trFRET) technique to measure the compaction of a set of peptides spanning the SOD1 sequence: the β1-β3 peptide (residues 1-36), the β4 peptide (residues 32-57), the Loop IV peptide (residues 58-86), the β5-β7 peptide (residues 87-120) and the Loop VII-β8 peptide (residues 121-153) (Fig. 1B and Materials and Methods). Three of these peptides were chosen on the basis of their resistance to proteolysis in *in vitro* and *in vivo* aggregates (24), supposing that these segments might be capable of nucleating aggregation reactions. The remaining two peptides, spanning residues 32-57 and 58-86, completed the set spanning the entire sequence. The peptides were purchased in pairs such that one of the pair contained only a single tryptophan (Trp) donor residue at or near one terminus, serving as the donor-only peptide (DO). The second member of the pair contained a tryptophan residue as well as a 5-((2-aminoethyl)amino)naphthalene-1-sulfonic

acid (EDANS) moiety conjugated to a glutamic acid residue at the other terminus, serving as the donor-acceptor peptide (DA). The Förster distance for Trp-EDANS is ~22 Å and is suitable for measuring the dimensions of peptides of these lengths.

FRET Efficiency from time-resolved fluorescence data

To test the state of compaction for each peptide we observed the excited state decay for each DO and DA pair as a function of denaturant using time-correlated single photon counting as previously described (25). We used Maximum Entropy Modeling (MEM) (26, 27) to fit these decays to rate distributions using the equation:

$$I_{DO/DA}(t) = \int p(k_d)e^{-k_d \cdot t} dk_d \qquad \text{(Eq. 1)}$$

where $I_{DO/DA}$ is the observed excited state decay for the DO or DA peptide, $p(k_d)$ is the distribution of excited-state decay rates, k_d is the donor decay rate constant and is also the inverse of the donor lifetime, $1/\tau$, and t is the time. From these distributions, we determined the quantum yield weighted average lifetime of the Trp, τ^{QY}, using the equation:

$$\tau^{QY} = \frac{\Sigma_i \alpha_i \tau_i^2}{\Sigma_i \alpha_i \tau_i} \qquad \text{(Eq. 2)}$$

where α is the amplitude associated with a distinct lifetime, τ, from the rate distribution. We then determined the quantum yield weighted averaged trFRET efficiency for each peptide and using the equation:

$$E_{trFRET} = 1 - \frac{\tau_{DA}^{QY}}{\tau_{DO}^{QY}} \qquad \text{(Eq. 3)}$$

Denaturant dependence of average trFRET efficiency

The quantum yield weighted average trFRET efficiency for the set of five peptides spanning the SOD1 sequence is plotted as a function of denaturant concentration in Fig. 2A. Strikingly, the trFRET efficiencies the Loop IV and Loop VII-β8 peptides were dependent on the urea concentration; the trFRET efficiencies of the remaining peptides were independent of the urea concentration. The trFRET efficiencies of both the Loop IV and Loop VII-β8 peptides decreased with increasing urea concentration. The decrease for the Loop VII-β8 peptide was distinctly nonlinear and

larger than that for the linear decrease for the Loop IV peptide. The expansion of the Loop VII-β8 peptide with denaturant is independent of the peptide concentration over the range from 2 to 20 μM, eliminating peptide-peptide interactions as an explanation for its behavior.

Noting that the β5-β6 segment, residues 82-102, forms a short β-hairpin in the native structure and was also found to be protected from proteolysis in *in vitro* aggregates (24), we examined the trFRET response of a peptide corresponding to this hairpin to increasingly denaturing environments (Fig. S1). This peptide was also found to be insensitive to denaturant.

As an independent test of the formation of structure in these peptides, we measured the far-UV CD spectra of each in the absence and presence of denaturant (Fig. S2). With the exception of the Loop VII-β8, the spectra in aqueous and denaturing conditions are coincident. We conclude that none of the other peptides formed detectable secondary structure.

The Loop VII-β8 peptide is unique in that the loop segment is of low complexity and polar, typical of an intrinsically disordered protein (28), while the β8 sequence is almost entirely nonpolar. To test the involvement of these distinctly different sequences at the termini of this peptide in its trFRET efficiency, we examined the behavior of two variants. One replaces isoleucine 149 in the β8 region with a threonine, an ALS-linked mutation that eliminates protection against proteolysis for *in vitro* aggregates of SOD1 (24). The other variant truncates five residues, EKADD, from the N-terminus (Fig. S3). We found that the trFRET efficiency for both variants in water is similar to that of the WT peptide in highly denaturing conditions (Fig. 2B). The trFRET efficiency for the I149T variant is independent of denaturant concentration while that of the truncated variant experiences a small linear decrease, similar to the behavior of the Loop IV peptide. Surprisingly, these results show that both the polar N- and nonpolar C-termini of the Loop VII-β8 peptide are involved in stabilizing the compact form of the peptide.

Gradual swelling or discrete unfolding?

The sensitivity of the trFRET efficiency to denaturant for the Loop IV and Loop VII-β8 peptides could reflect a gradual expansion from a

nonspecific collapsed state (29–31) or a two-state-like expansion from a discrete compact state to an expanded unfolded state (32). To resolve this issue, we utilized a two-dimensional form of Maximum Entropy Modeling (2DMEM)(25). 2DMEM is unbiased in that it makes no assumptions regarding the number of subpopulations or their lifetimes and allows for the possibility that each could have a distinct distance distribution (25). By analyzing our time-resolved fluorescence data with MEM, we can distinguish states that are resolved on the nanosecond time-scale. In 2DMEM, the raw excited state decays of the DO and DA peptides are globally fit using a 2D rate distribution matrix of donor decay, k_d and energy transfer, k_{ET}, rate constants using the following equations:

$$I_{DO}(t) = \int p(k_d)e^{-k_d \cdot t}dk_d \qquad (Eq. 1)$$

$$I_{DA}(t) = \iint p(k_d, k_{ET})e^{-(k_d+k_{ET}) \cdot t}dk_d k_{ET} \quad (Eq. 5)$$

There are two striking features in the results of the 2DMEM analysis of the Loop VII-β8 peptide (Fig. 3A). First there are multiple values of k_d and k_{ET} operative in the excited state decay. The three donor decay rate constants at 0.3, 1, and 8 ns^{-1} are characteristic of tryptophan (33), but only the slower two are FRET competent. The presence of both low and high FRET states with k_{ET} values of <1 and >1 ns^{-1}, respectively, indicate the presence of both expanded and compact states of the peptide. As the urea concentration increases, the population of the compact, high FRET state decreases while the population of the expanded, low FRET state increases in a concerted manner (Fig. 3B-3E). The results show that the change in trFRET efficiency for the Loop VII-β8 peptide reflects a two-state-like process between compact and expanded states separated by a kinetic barrier that is long relative to the nanosecond timescale of Trp excited-state decay. A denaturant-induced expansion of a randomly collapsed peptide would have produced a continuous shift of the high FRET state to the low FRET state. As a control, 2DMEM analysis of the β1-β3 peptide data in the absence of denaturant reveals only an expanded, low FRET state (Fig. 3F). The observation of a single donor decay rate constant for this peptide suggests that sequence differences in proximity to the indole side chain influence the rotamer distribution, which is often offered as an

explanation for the multiple lifetimes for Trp (34, 35). The β1-β3 peptide is unique among the examined peptides as the Trp donor is not at a terminus of the peptide, and the presence of residues before and after the Trp may give rise to the single lifetime distribution.

We also used 2DMEM analysis to examine the behavior of the Loop VII-β8 peptide variants in water (Fig. 4A-C). Neither the truncated nor the I149T variants were found to populate a compact, high FRET state, and both had trFRET efficiencies comparable to that for the WT Loop VII-β8 peptide under strongly denaturing conditions. We conclude that both the polar residues in the electrostatic loop and the nonpolar residues of β8 are involved in the formation of the compact state. The absence of a compact state for the truncated variant eliminates the possibility that other, intervening segments of the Loop VII-β8 peptide are involved in the compact state and indicates that the donor-acceptor probes do not drive the formation of the compact state.

We also used 2DMEM analysis to examine the Loop IV peptide in water and found that it does not populate a compact, high FRET state distinct from the expanded low FRET state (Fig. 4D). The continuous intensity from the low to high FRET region reflects the breadth of the conformational ensemble sampled by this peptide, and the small shift in response to increasing amounts denaturant (Fig. S4) is evidence that the change in trFRET observed in Fig. 2 reflects a gradual expansion of the molecule.

Dimensional analysis of the compact state for the Loop VII-β8 peptide in water

The energy transfer rate constant, k_{ET}, axis of the 2DMEM distributions (Fig. 3, 4 first panel) can be transformed into end-to-end distances through the Förster equation (see Materials and Methods). The transformation yields a matrix that provides the lifetime distribution of the donor residue, the end-to-end distance distribution for the peptide, as well as information about the donor lifetimes present in each ensemble of states. The result for the WT Loop VII-β8 peptide in the absence of denaturant is shown as a three-dimensional surface in Fig. 5, and the lifetime distribution of the Trp donor and the distance

distribution are projected along the XZ and YZ axes, respectively.

The lifetime distribution contains three peaks at ~0.3, ~1, and ~7 nanoseconds, in good agreement with typical complex lifetime distributions of Trp (33). The distance distribution shows a significant fraction of the population is compact with an end-to-end distance (R_{EED}) of ~14 Å that is only apparent from the two slower lifetimes. The conformational ensemble of the expanded state is very broad, with an estimated R_{EED} >30 Å. For reference, the expected R_{EED} for a random coil of 35 residues is ~45 Å (36).

Discussion
The C-terminus of SOD1 forms a compact state

Our trFRET data show that only the Loop VII-β8 peptide from SOD1 is capable of forming a compact thermodynamic state in water. The concerted transition from a compact to an expanded state with urea implies an intervening energy barrier; the sensitivity to urea reflects the burial of surface area from solvent, and the presence of comparable populations of the compact and expanded states are consistent with marginal stability ($\Delta G^0 \approx 0$ kcal/mol). The sensitivity of the compact state to the truncation of five residues (EKAAD) from the N-terminus and the I149T mutation near the C-terminus demonstrates their mutual involvement in its structure. These same segments are not in contact in the native conformation (Fig. 1A), suggesting that nonnative interactions are responsible for its formation. Interestingly, a peptide spanning residues 131-153 of SOD1 was used to develop an antibody recognizing misfolded, but not native, SOD1, consistent with our interpretation (37, 38).

One possibility for the nonnative structure is the formation of a β-hairpin by the nonpolar residues that form β8 and a pair of glycines at positions 27 and 30 that could enable a turn (see Experimental Procedures for the sequence). A small β-hairpin would explain the far-UV CD spectra observed for the Loop VII-β8 peptide in water (Fig. S2). This hairpin could serve to sequester the hydrophobic side chains from solvent and serve as a platform to interact with the polar residues at the N-terminus of the peptide.

Prior studies on the folding free energy surface of SOD1

Classic thermodynamic and kinetic studies of the folding of the monomeric chain of SOD1 have concluded that the reaction is well described by a two-state process, with a high barrier between the native and unfolded states (39). However, ensemble measurements may miss complexities that could appear in the folding of an individual chain. Woodside and colleagues have examined the folding free energy surface of a single molecule of SOD1 when subjected to a constant force exerted on the N- and C-termini (15). They found a complex set of partially-unfolded states that reflect the progressive unraveling of the β-sandwich architecture by the loss of individual β-strands. The initial step was the rupture of the β8 edge strand, and the final steps involved the disruption of structure in the β1-β2-β3 set of interlocking β-hairpins in one face of the sandwich and β4 in the opposing face. A contrasting view of the folding free energy surface of SOD1 in water at the individual amino acid level was obtained by hydrogen exchange (HDX) NMR spectroscopy (40). HDX-NMR is exquisitely sensitive to the presence of high-energy, partially-unfolded states of the sort predicted by the pulling experiments. The HDX-NMR results were consistent with a native basin defined by an intact β-sandwich, several of whose β-strands frayed at their termini. The majority of the main chain amide hydrogens in the β-strands exchanged in the unfolded state, i.e., not on the native side of the barrier to unfolding. There was no evidence for the partially-folded structures detected by the pulling experiment. Consistent with these results are those of kinetic folding studies of SOD1 by CD spectroscopy that did not detect the formation of secondary structure prior to the rate-limiting step in folding (20), i.e., on the unfolded side of the barrier to the native state. With the exception of the C-terminal peptide, the failure to detect compaction in peptides modeled after obvious elements of substructure in SOD1 in our trFRET experiments are in agreement with the HDX-NMR and CD studies. In other work, the partially-unfolded states observed by pulling experiments have been found to depend on the location of the tethers to exert the pulling force (41, 42). It remains to be seen how to relate the energy surfaces generated by pulling experiments on a single molecule with ensemble measurements

using hydrogen exchange or chemical denaturation.

A mechanism for the aggregation of SOD1 by the Loop VII-β8 segment

The >10 s lifetime of the unfolded state of SOD1 (39), prior to folding and maturation, would promote the formation of the compact structure at the C-terminus. A conceptual model for the mechanism by which this nonnative structure could lead to aggregation is shown in Fig. 6. The intrinsically long lifetime of the unfolded state combined with its being favored under physiological conditions by ALS mutations (19), provides an environment in which the intramolecular interactions in a single chain are replaced by intermolecular interaction between pairs of chains. These dimers could then progressively add chains to form a collection of soluble oligomers. The high local concentration of SOD1 chains in these oligomers would enhance the subsequent maturation to fibrils or amorphous aggregates. The observation that only the C-terminus is protected against proteolysis in aggregates extracted from mouse motor neurons suggests that this region is the primary driver of aggregation.

We used the aggregation prediction algorithms Aggrescan (43), WALTZ (44), and TANGO (45) to examine which of the peptides would be predicted to be prone to aggregation (Fig. S5). While two peptides, β4 and Loop IV, were predicted to have little or no aggregation prone stretches, the other peptides, β1-β3 and β5-β7 and Loop VII-β8, were predicted to have several regions that could be prone to aggregation. Interestingly, the only peptide where the three different algorithms show consensus is the Loop VII-β8 peptide and it is also the most hydrophobic region of the SOD1 sequence (46).

This mechanism does not account for the properties of the I149T mutation. I149T disrupts the compact structure in the C-terminus and eliminates protection against proteolysis for *in vitro* aggregates (24); however, it causes ALS. The observation that the β1-β3 and the β5-β6 segments are protected against proteolysis for *in vitro* aggregates of I149T shows that secondary nucleation sites come into play when the primary site is destabilized. Further support for alternative nucleation sites is the existence of the ALS-linked variants L126X, G127X, G141X, and C146X which truncate varying amounts of the C-terminus of SOD1 (5). The L126X variant was also shown to form *in vitro* aggregates with protection patterns similar to I149T (24). The existence of multiple pathways through which SOD1 can aggregate may also explain how different ALS-inked mutants give rise to morphologically distinct aggregates (47).

Another noteworthy element of the mechanism we propose is that it is not dependent upon the presence of an ALS-linked SOD1 mutation. The long lifetime of the unfolded chain, >10 sec, would provide an opportunity for the C-terminal region to sample the nonnative structure even in the WT-SOD1 background. The chain containing this nonnative structure could then be recognized by other misfolded protein partners, thereby providing an explanation for the recent observation of aggregated WT-SOD1 in tissue from patients with pathological ALS mutations in other genes (47).

Implications for therapeutic targets

The swap of intramolecular interactions for intermolecular interactions between C-terminal segments of unfolded SOD1 is the key step in the progression of events leading to soluble oligomers and macroscopic aggregation (Fig. 6). One therapeutic approach would be to screen for small molecules that preferentially stabilize the intramolecular, compact state and favor productive folding to the native dimer. Most ALS variants of SOD1 are extremely stable in their fully mature dimeric states (48, 49). An alternative approach, shown to be effective in non-human primates (50), would be to knockdown the expression of SOD1 with siRNAs and, thereby, slow the bimolecular steps crucial to the formation of soluble oligomers and aggregates. While not offering a cure for this tragic disease, these approaches or others might delay the onset and/or slow the progression of ALS.

Experimental Procedures
Peptide Design and Preparation

The peptides spanning the SOD1 sequence used in the FRET experiments were ordered form New England Peptide Inc., where the proper molecular weight was checked by mass spectrometry and the purity was ensured to be

>95% by HPLC. The sequences corresponding to the donor-only peptides follow:

β1-β3 peptide:
TKAVCVLKGDGPVQGIINFEQKESNGPVKVWGSIK
β4 peptide:
WGSIKGLTEGLHGFHVHEFGDNTAGC
Loop IV peptide:
WTSAGPHFNPLSRKHGGPKDEERHVGDLGN
β5-β7 peptide:
VTADKDGVADVSIEDSVISLSGDHCIIGRTLVVHW
Loop VII-β8 peptide:
EKADDLGKGGNEESTKTGNAGSRLACGVIGIAQW
I149T peptide:
EKADDLGKGGNEESTKTGNAGSRLACGVTGIAQW

Truncated peptide:
LGKGGNEESTKTGNAGSRLACGVTGIAQW
β5-β6 peptide:
GDLGNVTADKDGVADVSIEDSW

The donor-acceptor peptides are comprised of the same sequences with a Glu-EDANS moiety at the terminus opposite the Trp residue.

Small amounts (~1-2 mg) of the peptides were weighed out and resuspended in our experimental buffer: 20 mM 2-[4-(2-hydroxyethyl)piperazin-1-yl]ethanesulfonic acid, 1mM ethylenediaminetetraacetic acid, and 1 mM tris(2-carboxyethyl)phosphine at pH=7.2. Each peptide stock was filtered through a PES 0.22 μm filter and the concentrations were then determined using the 280 absorbance peak from the Trp donor (ε_{280}=5690 M^{-1}cm^{-1}) using a Cary 100-UV/Vis spectrophotometer. For the CD analysis, the same method was used, but the buffer used was 10 mM Potassium Phosphate, 1mM ethylenediaminetetraacetic acid, and 1 mM tris(2-carboxyethyl)phosphine at pH=7.2.

CD Spectroscopy

All CD measurements were performed with a Jasco-810 spectropolarimeter (Jasco Inc., Easton, MD) using a water-cooled Peltier unit. The spectra of a monomeric variant of SOD1 and the Loop VII-β8 and β1-β3 peptides from 190 to 260 nm were monitored using a quartz 0.1-cm path-length cuvette at a scan rate of 20 nm per min and an 8 second response time. The same methods were used to collect denatured spectra of the peptides, yet from only 215-260 nm to avoid scattering.

Time-Resolved FRET Measurements

The excitation was provided by the tripled output of a Ti:sapphire laser at 3.8 MHz repetition rate as previously described (25, 32). Excitation power was kept at several hundred μWatts at 292 nm. Counting rates in the detector channel were limited to 1×10^5 counts per second. A 357 nm 40 nm wide bandpass filter (Semrock, Rochester, NY) was used to select the Trp emission.

The samples were prepared from stocks of peptide in buffer and peptide in ≥ 6 M urea and mixed precisely using a Hamilton Microlab 500 titrator and in-house software. Equilibrium measurements were performed by interfacing a home-built autosampler running custom LabVIEW software (available at www.osmanbilsel.net) to the lifetime instrument. Each sample in a 96-well microplate was brought into a flow cell (1mm×1mm) using a Hamilton Microlab 560 dual syringe pump and flowed in an oscillating pattern at a flow rate of 10 μL/s during data collection. Doing so reduced continuous exposure of the sample to the beam to <1 sec and minimized photobleaching. An N-acetyl tryptophanamide (NATA) control was obtained prior to each titration in order to obtain relative quantum yields for all of the samples.

Maximum Entropy Modeling

Kumar *et al.* (27, 51) have shown that MEM can recover the distribution of decay rates from time-resolved data. To determine the trFRET values as a function of denaturant (Fig. 2A-2B), the excited-state decay of the Trp donor in the DO and DA peptides at each urea concentration were fit using Eq. 1. These distributions were used to calculate the quantum-yield weighted averaged lifetimes using Eq. 2 from which the trFRET efficiencies were calculated using Eq. 3.

The 2DMEM used to further analyze the time-resolved data used Eq. 1 and Eq. 5 to simultaneously fit the excited-state decays of the DO and DA samples, respectively. The fitting of all the MEM data was done with in-house software coded in LabVIEW (National Instruments) and available at https://osmanbilsel.net/software/. The $p(k_d, k_{ET})$ distributions were represented by 50×50 grids of rates in logarithmic rate space. No scaling of the DO and DA traces was used in the global fitting except in cases where a concentration

difference was known to be present. Additional terms accounting for scattered light and infinite time offsets were included in these analyses, but these were negligible and exclusion of these terms did not affect the resulting distributions.

These distributions were converted into efficiency histograms and distance distributions using another in-house software package that applies a quantum-yield correction to the R_0 of the donor-acceptor pair. The output of this software was then plotted in Fig. 5 as a three-dimensional surface of R_{EED}, k_d, and normalized Amplitude using the online open source software plot.ly. Two-dimensional projections of the R_{EED} *vs* normalized amplitude and k_d *vs* normalized amplitude distributions were also plotted along their respective axes.

Conflicts of Interest

The authors declare they have no conflicts of interest with the contents of this article.

REFERENCES

1.   Oskarsson, B., Gendron, T. F., and Staff, N. P. (2018) Amyotrophic Lateral Sclerosis: An Update for 2018. *Mayo Clin. Proc.* **93**, 1617–1628

2.   Redler, R. L., and Dokholyan, N. V (2012) The Complex Molecular Biology of Amyotrophic Lateral Sclerosis (ALS). *Prog. Mol. Biol. Transl. Sci.* **107**, 215–262

3.   Rosen, D. R., Siddique, T., Patterson, D., Figlewicz, D. A., Sapp, P., Hentati, A., Donaldson, D., Goto, J., O'Regan, J. P., Deng, H.-X., Rahmani, Z., Krizus, A., McKenna-Yasek, D., Cayabyab, A., Gaston, S. M., Berger, R., Tanzi, R. E., Halperin, J. J., Herzfeldt, B., Van den Bergh, R., Hung, W.-Y., Bird, T., Deng, G., Mulder, D. W., Smyth, C., Laing, N. G., Soriano, E., Pericak–Vance, M. A., Haines, J., Rouleau, G. A., Gusella, J. S., Horvitz, H. R., and Brown, R. H. (1993) Mutations in Cu/Zn superoxide dismutase gene are associated with familial amyotrophic lateral sclerosis. *Nature*. **362**, 59–62

4.   Valentine, J. S., Doucette, P. A., and Potter, S. Z. (2005) Copper-Zinc Superoxide Dismutase and Amyotrophic Lateral Sclerosis. *Annu. Rev. Biochem.* **74**, 563–93

5.   Abel, O., Powell, J. F., Andersen, P. M., and Al-Chalabi, A. (2012) ALSoD: A user-friendly online bioinformatics tool for amyotrophic lateral sclerosis genetics. *Hum. Mutat.* **33**, 1345–1351

6.   Ross, C. A., and Poirier, M. A. (2004) Protein aggregation and neurodegenerative disease. *Nat. Med.* **10**, S10–S17

7.   Chattopadhyay, M., and Valentine, J. S. (2009) Aggregation of Copper–Zinc Superoxide Dismutase in Familial and Sporadic ALS. *Antioxid. Redox Signal.* **11**, 1603–1614

8.   Ross, C. A., and Poirier, M. A. (2005) What is the role of protein aggregation in neurodegeneration? *Nat. Rev. Mol. Cell Biol.* **6**, 891–898

9.   Lelie, H. L., Liba, A., Bourassa, M. W., Chattopadhyay, M., Chan, P. K., Gralla, E. B., Miller, L. M., Borchelt, D. R., Valentine, J. S., and Whitelegge, J. P. (2011) Copper and zinc metallation status of copper-zinc superoxide dismutase from amyotrophic lateral sclerosis transgenic mice. *J. Biol. Chem.* **286**, 2795–806

10. Svensson, A.-K. E., Bilsel, O., Kayatekin, C., Adefusika, J. A., Zitzewitz, J. A., Matthews, C. R., and Hofmann, A. (2010) Metal-Free ALS Variants of Dimeric Human Cu,Zn- Superoxide Dismutase Have Enhanced Populations of Monomeric Species. *PLoS One*. **5**, 18–23

11. Oztug Durer, Z. A., Cohlberg, J. A., Dinh, P., Padua, S., Ehrenclou, K., Downes, S., Tan, J. K., Nakano, Y., Bowman, C. J., Hoskins, J. L., Kwon, C., Mason, A. Z., Rodriguez, J. A., Doucette, P. A., Shaw, B. F., and Valentine, J. S. (2009) Loss of Metal Ions, Disulfide Reduction and Mutations Related to Familial ALS Promote Formation of Amyloid-like Aggregates from Superoxide Dismutase. *PLoS One*. **4**, 5004

12. Furukawa, Y., and O'Halloran, T. V (2005) Amyotrophic lateral sclerosis mutations have the greatest destabilizing effect on the apo- and reduced form of SOD1, leading to unfolding and oxidative aggregation. *J. Biol. Chem.* **280**, 17266–74

13. Furukawa, Y., Kaneko, K., Yamanaka, K., O'Halloran, T. V, and Nukina, N. (2008) Complete loss of post-translational modifications triggers fibrillar aggregation of SOD1 in the familial form of amyotrophic lateral sclerosis. *J. Biol. Chem.* **283**, 24167–24176

14. Chattopadhyay, M., Nwadibia, E., Strong, C. D., Gralla, E. B., Valentine, J. S., and Whitelegge, J. P. (2015) The Disulfide Bond, but Not Zinc or Dimerization, Controls Initiation and Seeded Growth in Amyotrophic Lateral Sclerosis-linked Cu,Zn Superoxide Dismutase (SOD1) Fibrillation. *J. Biol. Chem.* **290**, 30624–36

15. Sen Mojumdar, S., Scholl, Z. N., Dee, D. R., Rouleau, L., Anand, U., Garen, C., and Woodside, M. T. (2017) Partially native intermediates mediate misfolding of SOD1 in single-molecule folding trajectories. *Nat. Commun.* **8**, 1881

16. Sekhar, A., Rumfeldt, J. A. O., Broom, H. R., Doyle, C. M., Bouvignies, G., Meiering, E. M., and Kay, L. E. (2015) Thermal fluctuations of immature SOD1 lead to separate folding and misfolding pathways. *Elife*. **4**, e07296

17. Sekhar, A., Rumfeldt, J. A. O., Broom, H. R., Doyle, C. M., Sobering, R. E., Meiering, E. M., and

Kay, L. E. (2016) Probing the free energy landscapes of ALS disease mutants of SOD1 by NMR spectroscopy. *Proc. Natl. Acad. Sci. U. S. A.* **113**, E6939–E6945

18. Culik, R. M., Sekhar, A., Nagesh, J., Deol, H., Rumfeldt, J. A. O., Meiering, E. M., and Kay, L. E. (2018) Effects of maturation on the conformational free-energy landscape of SOD1. *Proc. Natl. Acad. Sci.* **115**, E2546–E2555

19. Kayatekin, C., Zitzewitz, J. A., and Matthews, C. R. (2010) Disulfide-Reduced ALS Variants of Cu, Zn Superoxide Dismutase Exhibit Increased Populations of Unfolded Species. *J. Mol. Biol.* **398**, 320–331

20. Svensson, A. K. E., Bilsel, O., Kondrashkina, E., Zitzewitz, J. A., and Matthews, C. R. (2006) Mapping the Folding Free Energy Surface for Metal-free Human Cu,Zn Superoxide Dismutase. *J. Mol. Biol.* **364**, 1084–1102

21. Lang, L., Kurnik, M., Danielsson, J., and Oliveberg, M. (2012) Fibrillation precursor of superoxide dismutase 1 revealed by gradual tuning of the protein-folding equilibrium. *Proc. Natl. Acad. Sci. U. S. A.* **109**, 17868–73

22. Lang, L., Zetterström, P., Brännström, T., Marklund, S. L., Danielsson, J., and Oliveberg, M. (2015) SOD1 aggregation in ALS mice shows simplistic test tube behavior. *Proc. Natl. Acad. Sci.* **112**, 9878–9883

23. Ivanova, M. I., Sievers, S. a, Guenther, E. L., Johnson, L. M., Winkler, D. D., Galaleldeen, A., Sawaya, M. R., Hart, P. J., and Eisenberg, D. S. (2014) Aggregation-triggering segments of SOD1 fibril formation support a common pathway for familial and sporadic ALS. *Proc. Natl. Acad. Sci. U. S. A.* **111**, 197–201

24. Furukawa, Y., Kaneko, K., Yamanaka, K., and Nukina, N. (2010) Mutation-dependent polymorphism of Cu,Zn-superoxide dismutase aggregates in the familial form of amyotrophic lateral sclerosis. *J. Biol. Chem.* **285**, 22221–22231

25. Wu, Y., Kondrashkina, E., Kayatekin, C., Matthews, C. R., and Bilsel, O. (2008) Microsecond acquisition of heterogeneous structure in the folding of a TIM barrel protein. *Proc. Natl. Acad. Sci. U. S. A.* **105**, 13367–72

26. Skilling, J., and Bryan, R. K. (1984) Maximum entropy image reconstruction: general algorithm. *Mon. Not. R. astr. Soc*. **211**, 111–124

27. Livesey, A. K., and Brochon, J. C. (1987) Analyzing the Distribution of Decay Constants in Pulse-Fluorimetry Using the Maximum Entropy Method. *Biophys. J.* **52**, 693–706

28. Das, R. K., Ruff, K. M., and Pappu, R. V (2015) Relating sequence encoded information to form and function of intrinsically disordered proteins This review comes from a themed issue on Sequences and topology. *Curr. Opin. Struct. Biol.* **32**, 102–112

29. Kohn, J. E., Gillespie, B., and Plaxco, K. W. (2009) Non-Sequence-Specific Interactions Can Account for the Compaction of Proteins Unfolded under "Native" Conditions. *J. Mol. Biol.* **394**, 343–350

30. Chan, C. K., Hu, Y., Takahashi, S., Rousseau, D. L., Eaton, W. A., and Hofrichter, J. (1997) Submillisecond protein folding kinetics studied by ultrarapid mixing. *Proc. Natl. Acad. Sci. U. S. A.* **94**, 1779–84

31. Krantz, B. A., Mayne, L., Rumbley, J., Englander, S. W., and Sosnick, T. R. (2002) Fast and Slow Intermediate Accumulation and the Initial Barrier Mechanism in Protein Folding. *J. Mol. Biol.* **324**, 359–371

32. Kathuria, S. V., Kayatekin, C., Barrea, R., Kondrashkina, E., Graceffa, R., Guo, L., Nobrega, R. P., Chakravarthy, S., Matthews, C. R., Irving, T. C., and Bilsel, O. (2014) Microsecond Barrier-Limited Chain Collapse Observed by Time-Resolved FRET and SAXS. *J. Mol. Biol.* **426**, 1980–1994

33. Engelborghs, Y. (2001) The analysis of time resolved protein fluorescence in multi-tryptophan proteins. *Spectrochim. Acta Part A Mol. Biomol. Spectrosc.* **57**, 2255–2270

34. Bajzer, Z., and Prendergast, F. G. (1993) A Model for Multiexponential Tryptophan Fluorescence Intensity Decay in Proteins. *Biophys. J. Vol.* **65**, 2313–2323

35. Szabo, A. G., and Rayner, D. M. (1980) Fluorescence Decay of Tryptophan Conformers in Aqueous Solution. *J. Am. Chem. Soc.*

36. Goldenberg, D. P. (2003) Computational Simulation of the Statistical Properties of Unfolded Proteins. *J. Mol. Biol.* **326**, 1615–1633

37. Forsberg, K., Jonsson, P. A., Andersen, P. M., Bergemalm, D., Graffmo, K. S., Hultdin, M., Jacobsson, J., Rosquist, R., Marklund, S. L., and Brännström, T. (2010) Novel antibodies reveal inclusions containing non-native SOD1 in sporadic ALS patients. *PLoS One*. **5**, 11552

38. Forsberg, K., Andersen, P. M., Marklund, S. L., and Brännström, T. (2011) Glial nuclear aggregates of superoxide dismutase-1 are regularly present in patients with amyotrophic lateral sclerosis. *Acta Neuropathol.* **121**, 623–634

39. Kayatekin, C., Cohen, N. R., and Matthews, C. R. (2012) Enthalpic barriers dominate the folding and unfolding of the human Cu, Zn superoxide dismutase monomer. *J. Mol. Biol.* **424**, 192–202

40. Danielsson, J., Kurnik, M., Lang, L., and Oliveberg, M. (2011) Cutting off functional loops from homodimeric enzyme superoxide dismutase 1 (SOD1) leaves monomeric β-barrels. *J. Biol. Chem.* **286**, 33070–83

41. Guinn, E. J., Jagannathan, B., and Marqusee, S. (2015) Single-molecule chemo-mechanical unfolding reveals multiple transition state barriers in a small single-domain protein. *Nat. Commun.* **6**, 6861

42. Jagannathan, B., Elms, P. J., Bustamante, C., and Marqusee, S. (2012) Direct observation of a force-induced switch in the anisotropic mechanical unfolding pathway of a protein. *Proc. Natl. Acad. Sci. U. S. A.* **109**, 17820–17825

43. Conchillo-Solé, O., de Groot, N. S., Avilés, F. X., Vendrell, J., Daura, X., and Ventura, S. (2007) AGGRESCAN: a server for the prediction and evaluation of "hot spots" of aggregation in polypeptides. *BMC Bioinformatics*. **8**, 65

44. Maurer-Stroh, S., Debulpaep, M., Kuemmerer, N., Lopez de la Paz, M., Martins, I. C., Reumers, J., Morris, K. L., Copland, A., Serpell, L. C., Serrano, L., Schymkowitz, J. W. H., and Rousseau, F. (2010) Exploring the sequence determinants of amyloid structure using position-specific scoring matrices. *Nat. Methods*. **7**, 237–42

45. Fernandez-Escamilla, A.-M., Rousseau, F., Schymkowitz, J., and Serrano, L. (2004) Prediction of sequence-dependent and mutational effects on the aggregation of peptides and proteins. *Nat. Biotechnol.* **22**, 1302–6

46. Kyte, J., and Doolittle, R. F. (1982) A simple method for displaying the hydropathic character of a protein. *J. Mol. Biol.* **157**, 105–132

47. Forsberg, K., Graffmo, K., Pakkenberg, B., Weber, M., Nielsen, M., Marklund, S., Brännström, T., and Andersen, P. M. (2019) Misfolded SOD1 inclusions in patients with mutations in C9orf72 and other ALS/FTD-associated genes. *J. Neurol. Neurosurg. Psychiatry*. 10.1136/jnnp-2018-319386

48. Rodriguez, J. A., Valentine, J. S., Eggers, D. K., Roe, J. A., Tiwari, A., Brown, R. H., and Hayward, L. J. (2002) Familial amyotrophic lateral sclerosis-associated mutations decrease the thermal stability of distinctly metallated species of human copper/zinc superoxide dismutase. *J. Biol. Chem.* **277**, 15932–15937

49. Arnesano, F., Banci, L., Bertini, I., Martinelli, M., Furukawa, Y., and O'Halloran, T. V (2004) The unusually stable quaternary structure of human Cu,Zn-superoxide dismutase 1 is controlled by both metal occupancy and disulfide status. *J. Biol. Chem.* **279**, 47998–48003

50. Borel, F., Gernoux, G., Sun, H., Stock, R., Blackwood, M., Brown, R. H., and Mueller, C. (2018) Safe and effective superoxide dismutase 1 silencing using artificial microRNA in macaques. *Sci. Transl. Med.* **10**, eaau6414

51. Kumar, A. T. N., Zhu, L., Christian, J. F., Demidov, A. A., and Champion, P. M. (2001) On the rate distribution analysis of kinetic data using the maximum entropy method: Applications to myoglobin relaxation on the nanosecond and femtosecond timescales. *J. Phys. Chem. B*. **105**, 7847–7856

FOOTNOTES

The abbreviations used are: SOD1- Superoxide Dismutase 1, trFRET- time resolved FRET, trp-tryptophan, DO- donor-only, EDANS- 5-((2-aminoethyl)amino)naphthalene-1-sulfonic acid, DA- donor-acceptor, MEM- Maximum Entropy Modeling, 2DMEM- Two-dimensional Maximum Entropy Modeling, R_{EED}- end-to-end distance, HDX-NMR- Hydrogen exchange NMR, NATA- N-acetyl tryptophanamide,
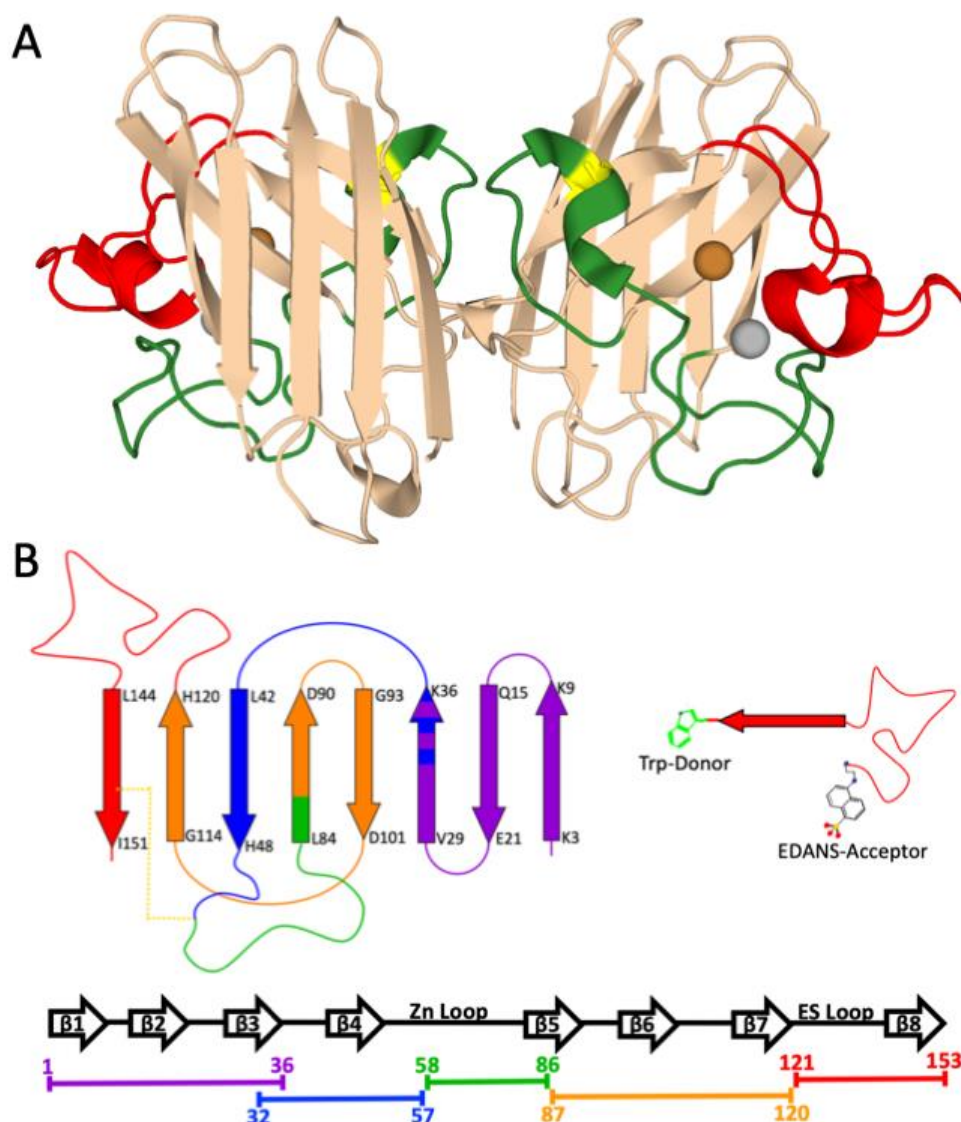
Figure 1. SOD1 Structure and Peptide Design. *A*, The ribbon diagram of Cu,Zn SOD1, adapted from PDB: 2C9V, is shown. The bound copper and zinc metal cofactors are shown as orange and grey spheres, and the internal disulfide bond is shown in yellow. The zinc binding and electrostatic loops are shown in green and red, respectively. *B*, Each of the examined peptides of SOD1 is mapped onto the topology diagram with a unique color in the top left. A sketch demonstrating how the FRET donors and acceptors were placed onto the termini of one of the peptides is shown on the top right. The exact residue length of each peptide is shown along a linear map of the SOD1 structure using the same colors as in the topology map above. The colors associated with each peptide are carried forward to Figure 2.

13
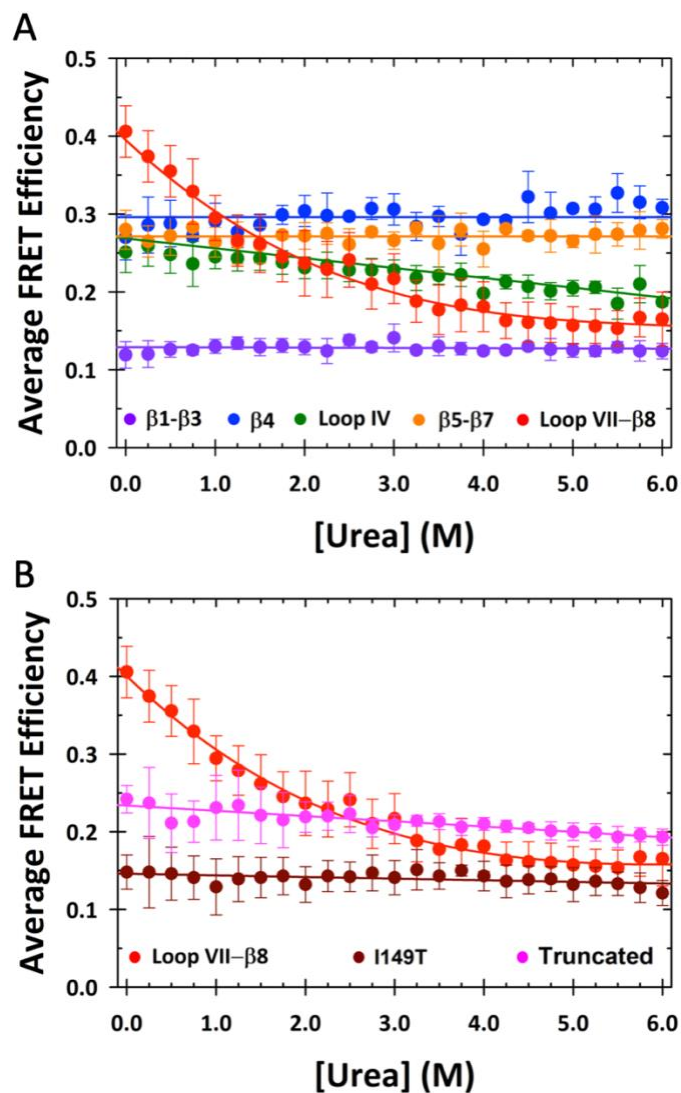
Figure 2: trFRET efficiency of SOD1 peptides as a function of denaturant. *A*, The quantum yield weighted average trFRET efficiencies for each of the five SOD1 peptides are shown as a function of denaturant (colors as in Figure 1B), and trend lines are shown to demonstrate the linearity or nonlinearity of the FRET change for each peptide. *B*, The FRET efficiencies for the Loop VII-β8 peptide (red) and the I149T (maroon) and truncated (pink) variants are shown as a function of denaturant and trend lines are shown to demonstrate the linearity or nonlinearity of the FRET change for each peptide. The data points represent the average of ≥3 separate experimental runs, and the error bars are the standard deviation thereof.
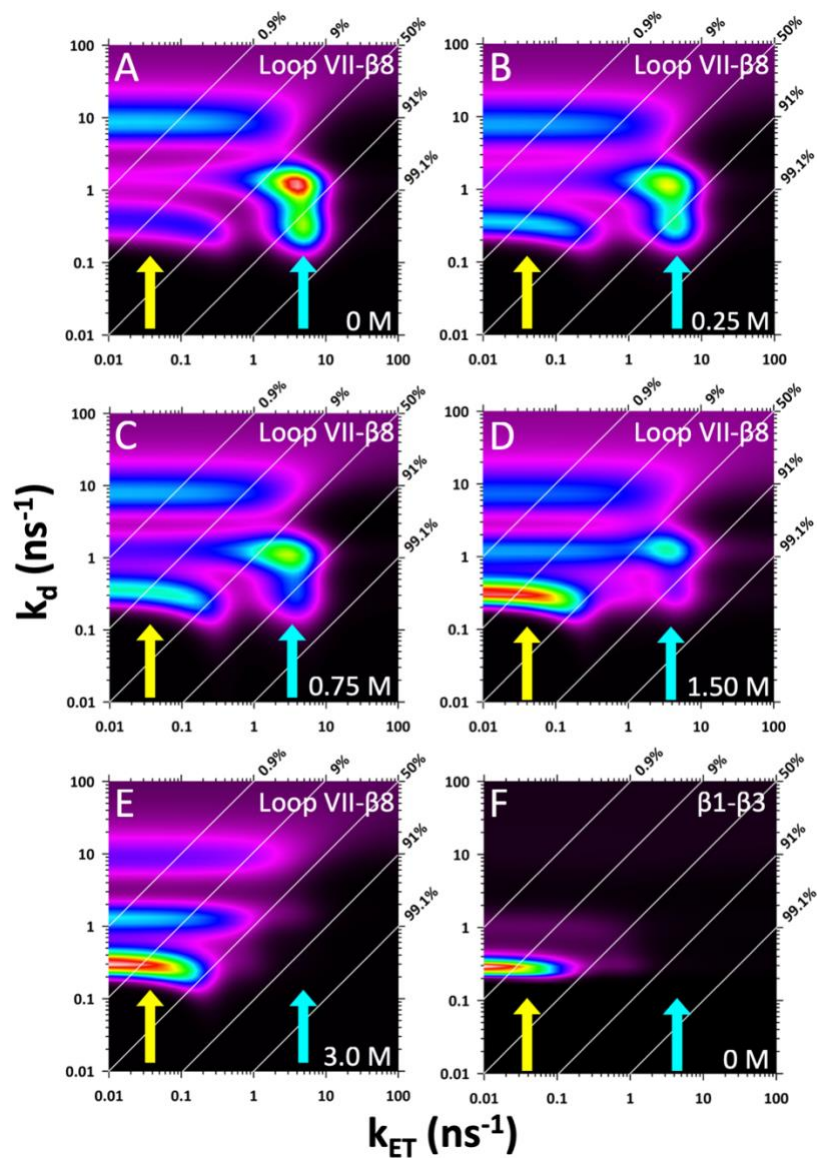
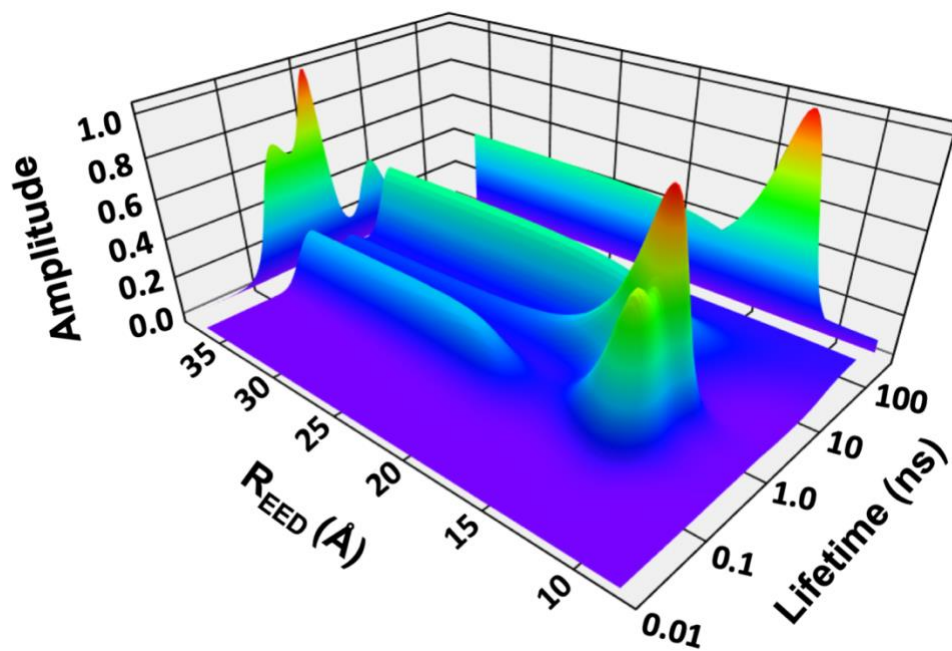**Figure 3. 2DMEM distributions for the Loop VII-β8 peptide as a function of denaturant.** *A-E*, The concentrations of urea examined are shown in the lower right corners of each panel, and the upper right corner of each panel is labeled with the examined peptide. The amplitude of the distributions in *B-E* was normalized to the amplitude in *A* to emphasize the change in response to denaturant. *F*, The 2DMEM distribution for the β1-β3 peptide in the absence of denaturant is shown for reference. The diagonal white reference lines are marked with the FRET efficiency along each line. The yellow arrows indicate the amplitude associated with extended conformations, and the cyan arrows indicate the amplitude associated with compact conformations.

15
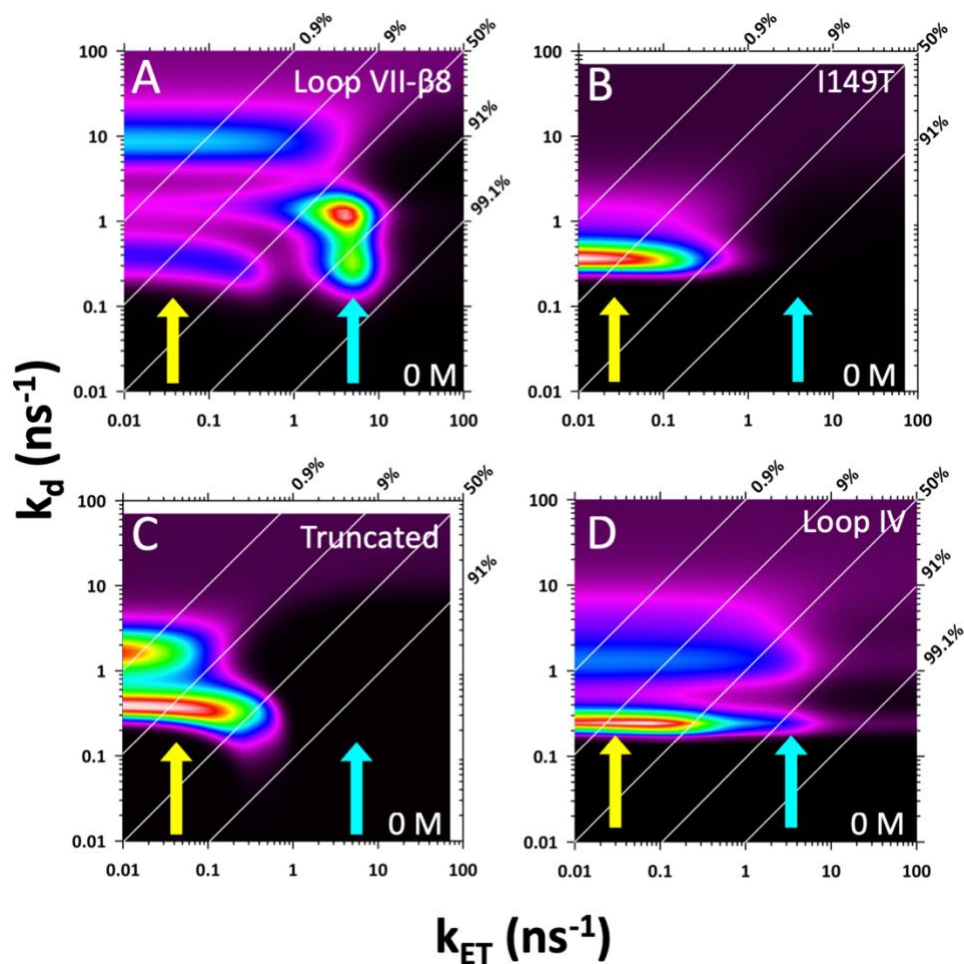
Figure 4. The 2DMEM distributions for the Loop VII-β8 peptide variants. The concentrations of urea examined are shown in the lower right corners of each panel, and the upper right corner of each panel is labeled with the examined peptide. The diagonal white reference lines are marked with the FRET efficiency along each line. The yellow arrows indicate the amplitude associated with extended conformations, and the cyan arrows indicate the amplitude associated with compact conformations.

Figure 5. Three-dimensional surface of the transformed 2DMEM distribution for the WT Loop VII-β8 peptide in the absence of denaturant. The two-dimensional Trp lifetime distribution and the end-to-end distance distribution are shown as projections along the XZ and YZ axes, respectively.
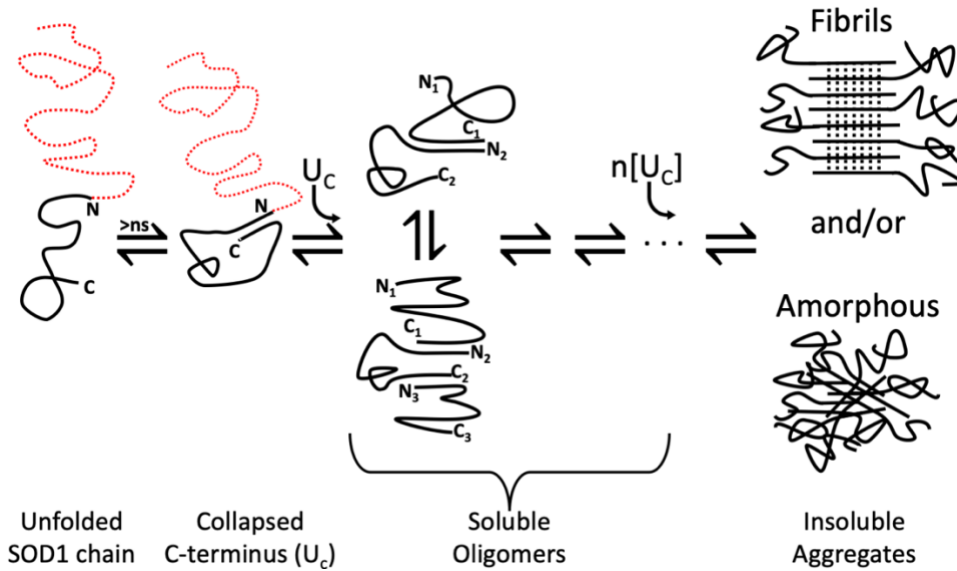
Figure 6. A model for the role of the compact Loop VII-β8 region in ALS-linked SOD1 aggregation.
In this model, the C-terminal region (black line) is able to form the compact state, while the rest of the polypeptide chain remains unfolded (red dotted line). Once the compact state has formed, it can meet other compact states and form lower order, soluble oligomers. These oligomers could then further recruit polypeptide chains until insoluble aggregates, either fibril-like or amorphous, are formed.

Nonnative structure in a peptide model of the unfolded state of SOD1: Implications for ALS-linked aggregation

Noah R. Cohen, Jill Ann Zitzewitz, Osman Bilsel and C. Robert Matthews

Access the most updated version of this article at doi: 10.1074/jbc.RA119.008765

Alerts:
- When this article is cited
- When a correction for this article is posted

Click here to choose from all of JBC's e-mail alerts